Quantum critical point in the superconducting transition on the surface of a topological insulator

Dingping Li,[1,2,*] Baruch Rosenstein,[3,4,†] B. Ya. Shapiro,[5,‡] and I. Shapiro[5]
[1]*School of Physics, Peking University, Beijing 100871, China*
[2]*Collaborative Innovation Center of Quantum Matter, Beijing 100871, China*
[3]*Electrophysics Department, National Chiao Tung University, Hsinchu 30050,* Taiwan
[4]*Physics Department, Ariel University, West Bank*
[5]*Physics Department, Bar-Ilan University, 52900 Ramat-Gan, Israel*
(Received 2 May 2014; revised manuscript received 19 July 2014; published 25 August 2014)

Pairing in the Weyl semimetal appearing on the surface of a topological insulator is considered. It is shown that due to an "ultrarelativistic" dispersion relation there is a quantum critical point governing the zero-temperature transition to a superconducting state. Starting from the microscopic Hamiltonian with local attraction, we calculated using the Gor'kov equations, the phase diagram of the superconducting transition at arbitrary chemical potential, and its magnetic properties and critical exponents close to the quantum critical point. The Ginzburg-Landau (GL) effective theory is derived for small chemical potential, allowing us to consider effects of spatial dependence of order parameters in a magnetic field. The GL equations are very different from the conventional ones reflecting the chiral universality class of the quantum phase transition. The order-parameter distribution of a single vortex is found to be different as well. The magnetization near the upper critical field is found to be quadratic, not linear as usual. We discuss the application of these results to recent experiments in which surface superconductivity was found for some three-dimensional topological insulators, and we estimate feasibility of the phonon pairing.

DOI: 10.1103/PhysRevB.90.054517 PACS number(s): 74.20.Fg, 74.90.+n, 74.20.De

I. INTRODUCTION

A topological insulator (TI) is a novel state of matter in materials with strong spin-orbit interactions that create topologically protected surface states [1]. The electrons (holes) in these states have a linear dispersion relation and can be described approximately by a (pseudo) relativistic two-dimensional (2D) Weyl Hamiltonian. The system with the chemical potential above or below the Weyl point realizes an "ultrarelativistic" 2D electron or hole conducting liquid. It has been known for a long time that similar 2D and quasi-2D metallic systems, like the surface metal on twin planes [2] and layered materials (strongly anisotropic high T_c cuprates [3] or organic superconductors [4]), may develop 2D (surface) superconductivity. This phenomenon became known as "localized superconductivity" [5]. Since the most studied TIs possess a quite standard phonon spectrum [6], it was predicted recently [7] that they become superconducting TIs (STIs) [this should be distinguished from "topological superconductors" (TSCs), in which superconductivity appears in the bulk [1]]. The predicted critical temperature of 1 K is rather low (despite a fortunate suppression of the Coulomb repulsion due to a large dielectric constant $\varepsilon \sim 50$); the nature of the "normal" state (the so-called 2D Weyl semimetal) might make the superconducting properties of the system unusual. The ultrarelativistic nature manifests itself mostly when the Weyl cone is very close to the Fermi surface. Especially interesting is the case (originally predicted for the [111] surface of Bi_2Te_3 and Bi_2Se_3 [8]) when the chemical potential coincides with the Weyl point. Although subsequent angle-resolved photoemission spectroscopy experiments [1] show the location of the cone of surface states to be on the order of tenths of eV off the Fermi surface, there are experimental means to shift the chemical potential, for example, by the bias voltage [9].

Unlike the more customary poor 2D metals with several small pockets of electrons or holes on the Fermi surface (in semiconductor systems or even some high T_c materials [3]), the electron gas STI has two peculiarities that are especially important when pairing is contemplated. The first is the bipolar nature of the Weyl spectrum: there is no energy gap between the upper and lower cones. The second is that the spin degree of freedom is a major player in the quasiparticle dynamics. This degree of freedom determines the pairing channel. The pairing channel problem was studied theoretically on the level of the Bogoliubov-de Gennes equation [10]. Both s and p waves are possible and compete due to the breaking of the bulk inversion symmetry by the surface. The spectrum of Andreev states of the Abrikosov vortex was obtained [11] in a related problem of a TI in contact with an s-wave superconductor [12]. Various pairing interactions were considered to calculate the density of states measured in $Cu_xBi_2Se_3$ to discriminate between STIs and TSCs using self-consistent analysis [13]. As mentioned above the most intriguing case is that of the small chemical potential that has not been addressed microscopically. It turns out that it is governed by a quantum critical point (QCP) [14].

The concept of a QCP at zero temperature and varying doping constitutes a very useful language for describing the microscopic origin of superconductivity in high T_c cuprates and other "unconventional" superconductors [3] . Superconducting transitions generally belong to the $U(1)$ class of second-order phase transitions [15], however it was pointed out a long time ago [16] that, if the normal state dispersion relation is ultrarelativistic, the transition at zero temperature as a function of parameters like the pairing interaction strength

*lidp@pku.edu.cn
†Corresponding author: vortexbar@yahoo.com
‡shapib@mail.biu.ac.il

is qualitatively distinct and belongs to chiral universality classes classified in [17]. Attempts to experimentally identify second-order transitions governed by a QCP included quantum magnets [14], superconductor-insulator transitions [18], and more recently chiral condensates in graphene [19,20].

In this paper we study the thermodynamic and magnetic properties of the surface superconductivity in a TI with local attraction, pairing a Hamiltonian characterized by the coupling strength g and cutoff parameter T_D within the self-consistent approximation. The phase diagram for s-wave pairing is obtained for arbitrary temperature T and chemical potential $\mu < T_D$. The latter condition is the main difference from the conventional BCS model in which $\mu \gg T_D$. We found a quantum critical point at $T = \mu = 0$ when the coupling strength g reaches a critical value g_c dependent on the cutoff parameter. We concentrate on properties of the superconducting state in a part of the phase diagram that is dominated by the QCP. Various critical exponents are obtained. In particular, the coupling strength dependence of the coherence length is $\xi \propto (g - g_c)^{-\nu}$ with $\nu = 1$, and the order parameter scales as $\Delta \propto (g - g_c)^{\beta}$, $\beta = 1$. It is found that near the QCP the Ginzburg-Landau (GL) effective model is rather unconventional. The structure of the single vortex core is different from the usual Abrikosov vortex, while the magnetization curve near the upper critical magnetic field H_{c2} is quadratic: $M = (H - H_{c2})^2$, not linear.

The rest of the paper is organized as follows. The model and the method of its solution (in the Gor'kov equations form) are presented in Sec. II. The phase diagram in the homogeneous case (no magnetic field) is established, and the unusual nature of the phase transition is discussed. The novel case of zero chemical potential (tuning to the Weyl point) is studied in detail. The Ginzburg-Landau energy is derived in Sec. III and exploited to determine magnetic properties of STIs. The H_{c2} line and magnetization curves for a dense vortex lattice as well as the single vortex texture are obtained. Section IV contains discussion on experimental feasibility of the phonon mediated surface superconductivity in TIs, comparison with more familiar Bose-Einstein condensate (BEC) and BCS scenarios, and conclusion.

II. THE s-WAVE PAIRING MODEL: THE PHASE DIAGRAM

A. TI in magnetic field with a local pairing interaction: Gor'kov equations

Electrons on the surface of a TI perpendicular to the z axis (see Fig. 1) are described by a Pauli spinor $\psi_\alpha(\mathbf{r})$, where the upper plane, $\mathbf{r} = \{x, y\}$, is considered, with spin projections taking the values $\alpha = \uparrow, \downarrow$ with respect to the z axis. The Hamiltonian for electrons in a TI subjected to a perpendicular external homogeneous magnetic field, and interacting via a four-Fermi local coupling of strength g, is

$$H = \int d^2r \left\{ \psi^+_\alpha(\mathbf{r}) \widehat{H}_{\alpha\beta} \psi_\beta(\mathbf{r}) - \frac{g}{2} \psi^+_\alpha(\mathbf{r}) \psi^+_\beta(\mathbf{r}) \psi_\beta(\mathbf{r}) \psi_\alpha(\mathbf{r}) \right\} + H_{\rm mag}. \quad (1)$$

Here the surface Weyl Hamiltonian matrix [1,10] is defined as

$$\widehat{H}_{\alpha\beta} = v_F \varepsilon_{ij} \widehat{P}_i \sigma^j_{\alpha\beta} - \mu \delta_{\alpha\beta}, \quad (2)$$

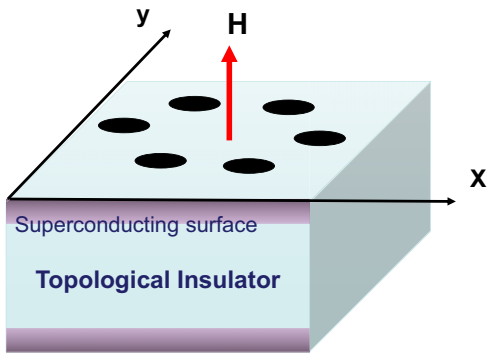

FIG. 1. (Color online) Topological insulator plate in magnetic field. Surfaces are populated by Weyl quasiparticles and holes that both can be paired by interactions. The magnetic field creates vortices with normal cores (dark areas on the surfaces) of the radius of order of coherence length ξ.

$$\widehat{\mathbf{P}} \equiv -i\hbar\nabla - \frac{e^*}{c}\mathbf{A}(\mathbf{r}),$$

where $i, j = x, y$; v_F is the Fermi velocity of the TI; and μ is the surface chemical potential. σ^j are the Pauli matrices, and ε_{ij} is the antisymmetric tensor. Only one valley is explicitly considered (generalization to several "flavors" is trivial). Vector potential $\mathbf{A}$ describes the three-dimensional (3D) magnetic induction $\mathbf{B} = \nabla \times \mathbf{A}$ with magnetic energy given by

$$H_{\rm mag} = \frac{1}{8\pi} \int d^2r dz \left[\mathbf{B}(\mathbf{r}, z) - \mathbf{H}_{\rm ext}\right]^2. \quad (3)$$

The effective local interaction might be generated by a phonon exchange or perhaps other mechanisms and will be assumed to be weak coupling. Therefore the BCS type approximation can be employed. Using the standard formalism, the Matsubara Green's functions (τ is the Matsubara time),

$$\begin{aligned} G_{\alpha\beta}(\mathbf{r}, \tau; \mathbf{r}', \tau') &= -\langle T_\tau \psi_\alpha(\mathbf{r}, \tau) \psi^\dagger_\beta(\mathbf{r}', \tau') \rangle, \\ F^\dagger_{\alpha\beta}(\mathbf{r}, \tau; \mathbf{r}', \tau') &= \langle T_\tau \psi^\dagger_\alpha(\mathbf{r}, \tau) \psi^\dagger_\beta(\mathbf{r}', \tau') \rangle, \end{aligned} \quad (4)$$

obey the Gor'kov equations [21]:

$$\begin{aligned} &-\frac{\partial G_{\gamma\kappa}(\mathbf{r}, \tau; \mathbf{r}', \tau')}{\partial \tau} - \int_{\mathbf{r}''} \langle \mathbf{r} | \widehat{H}_{\gamma\beta} | \mathbf{r}'' \rangle G_{\beta\kappa}(\mathbf{r}'', \tau; \mathbf{r}', \tau') \\ &\quad - g F_{\beta\gamma}(\mathbf{r}, \tau; \mathbf{r}, \tau) F^\dagger_{\beta\kappa}(\mathbf{r}, \tau, \mathbf{r}', \tau') = \delta^{\gamma\kappa} \delta(\mathbf{r} - \mathbf{r}') \delta(\tau - \tau'), \\ &\frac{\partial F^\dagger_{\gamma\kappa}(\mathbf{r}, \tau; \mathbf{r}', \tau')}{\partial \tau} - \int_{\mathbf{r}''} \langle \mathbf{r} | \widehat{H}^t_{\gamma\beta} | \mathbf{r}'' \rangle F^\dagger_{\beta\kappa}(\mathbf{r}'', \tau; \mathbf{r}', \tau') \\ &\quad - g F^\dagger_{\gamma\beta}(\mathbf{r}, \tau; \mathbf{r}, \tau) G_{\beta\kappa}(\mathbf{r}, \tau, \mathbf{r}', \tau') = 0. \end{aligned} \quad (5)$$

In the presence of a magnetic field these equations are complicated by emergence of inhomogeneity pertinent to type-II superconductors. This will be addressed in Sec. III. Here we solve the homogeneous case when no magnetic field is present.

B. Uniform condensate

In the homogeneous case the Gor'kov equations for Fourier components of the Green's functions simplify considerably:

$$\begin{aligned} D^{-1}_{\gamma\beta} G_{\beta\kappa}(\omega,p) - \widehat{\Delta}_{\gamma\beta} F^{\dagger}_{\beta\kappa}(\omega,p) &= \delta^{\gamma\kappa}, \\ D^{-1}_{\beta\gamma} F^{\dagger}_{\beta\kappa}(\omega,p) + \widehat{\Delta}^{*}_{\gamma\beta} G_{\beta\kappa}(\omega,p) &= 0, \end{aligned} \tag{6}$$

where $\omega = \pi T(2n+1)$ is the Matsubara frequency and $D^{-1}_{\gamma\beta} = (i\omega - \mu)\delta_{\gamma\beta} - v_F \varepsilon_{ij} p_i \sigma^{j}_{\alpha\beta}$. The matrix gap function can be chosen as (Δ real)

$$\widehat{\Delta}_{\beta\gamma} = g F_{\gamma\beta}(0) = \begin{pmatrix} 0 & \Delta \\ -\Delta & 0 \end{pmatrix}. \tag{7}$$

These equations are conveniently presented in matrix form (superscript t denotes transposition, and I denotes the identity matrix):

$$\begin{aligned} D^{-1} G - \widehat{\Delta} F^{\dagger} &= I, \\ D^{t-1} F^{\dagger} + \widehat{\Delta}^{*} G &= 0. \end{aligned} \tag{8}$$

Solving these equations, one obtains

$$\begin{aligned} G^{-1} &= D^{-1} + \widehat{\Delta} D^{t} \widehat{\Delta}^{*}, \\ F^{\dagger} &= -D^{t} \widehat{\Delta}^{*} G, \end{aligned} \tag{9}$$

with the gap function found from the consistency condition:

$$\widehat{\Delta}^{*} = -g \sum_{\omega q} D^{t} \widehat{\Delta}^{*} G. \tag{10}$$

The off-diagonal component of this equation is

$$\Delta = g\Delta \sum_{\omega q} \left(\Delta^2 + v_F^2 p^2 + \mu^2 + \hbar^2\omega^2\right) \times \frac{1}{(\Delta^2 + \hbar^2\omega^2 + (v_F p - \mu)^2)(\Delta^2 + \hbar^2\omega^2 + (v_F p + \mu)^2)}. \tag{11}$$

The spectrum of elementary excitations obtained from the poles of the Green's function coincides with that found within the Bogoliubov-de Gennes approach [10]:

$$E_p = \pm\sqrt{\Delta^2 + (v_F p - \mu)^2}. \tag{12}$$

The solutions of the gap equation are presented in the next subsection for a general chemical potential and zero temperature, while more general situations (arbitrary temperature and magnetic field) in the most interesting case of $\mu = 0$ are addressed in the next section.

C. Zero-temperature phase diagram and QCP

At zero temperature the integrations over frequency and momentum limited by the UV cutoff Λ result in (see Appendix A for details)

$$U\Delta = \Delta\left(\sqrt{\Delta^2 + \mu^2} - \frac{\mu}{2}\log\frac{\sqrt{\Delta^2+\mu^2}+\mu}{\sqrt{\Delta^2+\mu^2}-\mu}\right), \tag{13}$$

where the dependence on the cutoff is incorporated in the renormalized coupling with the dimension of energy defined as

$$U = v_F\Lambda - \frac{4\pi\hbar^2 v_F^2}{g}. \tag{14}$$

This can be interpreted as an effective binding energy of the Cooper pair in the Weyl semimetal. For concreteness we consider only $\mu > 0$, although the particle-hole symmetry makes the opposite case of the hole doping, $\mu < 0$, identical. Of course the superconducting solution exists only for $g > 0$. In Fig. 2 the dependence of the gap Δ as a function of the chemical potential μ is presented for different values of U.

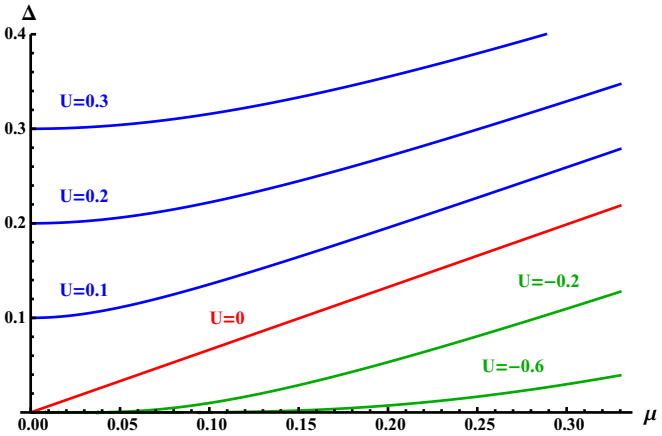

FIG. 2. (Color online) Order parameter at zero temperature as a function of chemical potential of the TI surface Weyl semimetal at various values of coupling parametrized by the renormalized energy U, Eq. (14). For positive U (blue lines) the superconductivity is strong and does not vanish even for zero chemical potential. There exists the critical coupling, $U = 0$ (the red line), at which the second-order transition occurs at quantum critical point $\mu = 0$. For negative U the superconductivity still exists at $\mu > 0$ but is exponentially weak.

For an attractive coupling g stronger than the critical one,

$$g_c = \frac{4\pi\hbar^2 v_F}{\Lambda} \tag{15}$$

(when $U > 0$, blue lines in Fig. 2), there are two qualitatively different cases.

(1) When $\mu \ll U$ the dependence of Δ on the chemical potential is parabolic (see Appendix B):

$$\frac{\Delta}{U} \approx 1 + \left(\frac{\mu}{U}\right)^2. \tag{16}$$

In particular, when $\mu = 0$, the gap equals U. As can be seen from Fig. 2, the chemical potential makes a very limited impact in the large portion of the phase diagram.

(2) For the attraction just stronger than critical—$g > g_c$, namely, for small positive U—the dependence becomes linear (see the red line in Fig. 2), $\Delta = 0.663\,\mu$. So that the already weak condensate becomes sensitive to μ.

Case 1 is more interesting than case 2, since it exhibits stronger superconductivity (larger T_c, see below). Finally, for $g < g_c$, namely, negative U (green lines in Fig. 2), the superconductivity is very weak with exponential dependence similar to the BCS one:

$$\Delta \approx \mu \exp[-(|U|/\mu - 1)]. \tag{17}$$

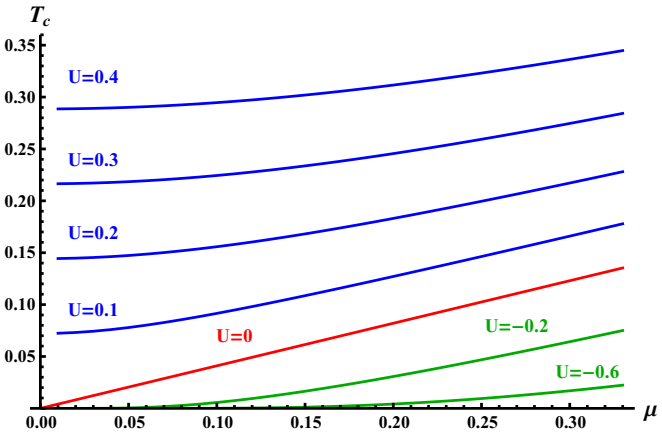

FIG. 3. (Color online) Transition temperature as a function of chemical potential at supercritical ($U > 0$, in blue), critical ($U = 0$, in red), and subcritical values of coupling.

More detailed comparisons will be performed in Sec. IV. As was mentioned above, in the more interesting cases of large Δ the dependence on the chemical potential is very weak. A peculiarity of superconductivity in TIs is that electrons (and holes) in Cooper pairs are created themselves by the pairing interaction rather than being present in the sample as free electrons. Therefore it is shown that it is possible to neglect the effect of weak doping and consider directly the $\mu = 0$ particle-hole symmetric case. This point in parameter space is the QCP [14] and will be studied in detail in what follows. Of course, at finite temperature at any attraction, $g > 0$, there exists a (classical) superconducting critical point at certain temperature T_c, calculated next.

D. Dependence of the critical temperature T_c on strength of pairing interaction

Summation over Matsubara frequency and integrations over momenta in the gap equation, Eq. (13), at finite temperature and arbitrary chemical potential are performed in Appendix B. The critical temperature as a function of μ and (positive) U is obtained numerically and presented in Fig. 3. Again at relatively large U the dependence of T_c on the chemical potential is very weak and parabolic. When $0 < g < g_c$ the critical temperature is exponentially small albeit nonzero.

E. Zero chemical potential $\mu = 0$

At zero chemical potential the Hamiltonian Eq. (1) possesses a particle-hole symmetry. Microscopically, Cooper pairs of both electrons and holes are formed. The system is unique in this sense since the electron-hole symmetry is not spontaneously broken in both normal and superconducting phases. The supercurrent in such a system does not carry momentum or mass. Performing the sum and integral over momenta in the gap equation, Eq. (13), analytically (see Appendix A), it becomes [using the definition of U given in Eq. (14)] for $U > 0$

$$U = 2T \log\left[2\cosh\frac{\Delta}{2T}\right]. \tag{18}$$

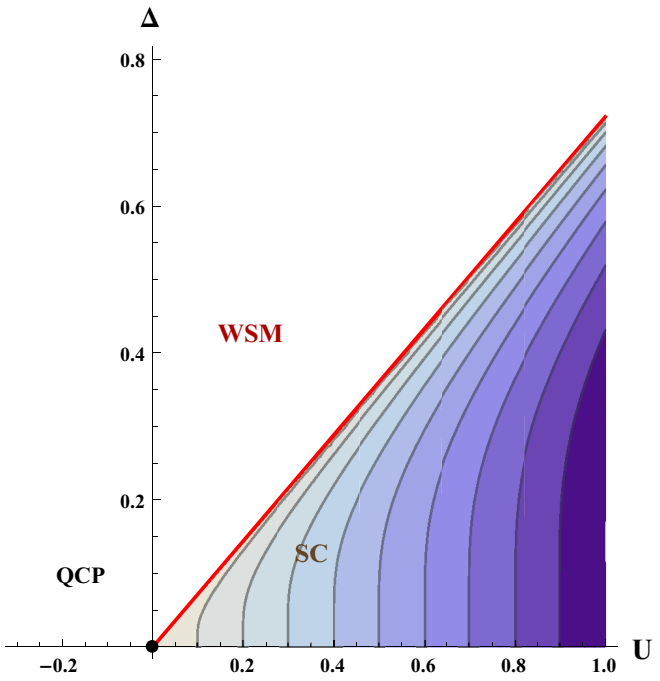

FIG. 4. (Color online) Phase diagram of the STI and order parameter as a function of U describing the deviation from criticality near the quantum critical point at $\Delta = 0$, $\mu = 0$. The critical line is a straight line in mean-field approximation.

At zero temperature $\Delta = U$, while $\Delta \to 0$ as a power of the parameter $U \propto g - g_c$, describing the deviation from quantum criticality:

$$T_c = \frac{1}{2\log 2} U^{z\nu}, \quad z\nu = 1. \tag{19}$$

Here z is the dynamical critical exponent [14]. Therefore, as expected, the renormalized coupling describing the deviation from the QCP is proportional to the temperature at which the created condensate disappears.

The temperature dependence of the gap reads (see Fig. 4)

$$\Delta(T) = 2T \cosh^{-1}\left(\frac{1}{2}\exp\frac{U}{2T}\right). \tag{20}$$

This it typical for chiral universality classes [14,16].

It is interesting to compare this dependence with the conventional BCS for transition at finite temperature, namely, away from the QCP. At zero temperature $\Delta(0)/T_c = 2\log 2 = 1.39$ (within BCS, 1.76), while near T_c one gets $\Delta/T_c = 2^{3/2}\log^{1/2} 2\sqrt{1-t} = 2.35\sqrt{1-t}$ (within BCS, $3.07\sqrt{1-t}$), where $t = T/T_c$. To describe the behavior of the STI in inhomogeneous situations like the external magnetic field, boundaries, impurities, or junction with metals or other superconductors, it is necessary to derive the effective theory in terms of the order parameter $\Delta(\mathbf{r})$, where $\mathbf{r}$ varies on the mesoscopic scale.

III. GINZBURG-LANDAU EFFECTIVE THEORY AND MAGNETIC PROPERTIES OF THE SUPERCONDUCTOR NEAR QCP

A. Coherence length and the condensation energy

Using the well-known Gor'kov method [21], the quadratic term of the Ginzburg-Landau energy $F_2 = \sum_{\mathbf{p}} \Delta_p^* \Gamma(p) \Delta_p$ is obtained exactly from expanding the gap equation to linear terms in Δ for arbitrary external momentum. The result derived in Appendix B reads

$$\Gamma(p) = -\frac{U}{4\pi\hbar^2 v_F^2} + \frac{|p|}{16 v_F \hbar^2}. \tag{21}$$

The dependence on $\mathbf{p}$ is nonanalytic, and within our approximation higher powers of p do not appear. The second term is very different from the quadratic term in the GL functional for conventional phase transitions at finite temperature [15] or even quantum phase transitions in models without Weyl fermions [14] and has a number of qualitative consequences. Comparing the two terms in Eq. (21), one obtains the coherence length as a power of parameter $U \propto g - g_c$ describing the deviation from criticality:

$$\xi(U) = \frac{\pi}{4} v_F \hbar U^{-\nu}, \quad \nu = 1. \tag{22}$$

This is different from the dependence in nonchiral universality classes that is [15] $\xi(T) \infty (T_c - T)^{-\nu}$, $\nu = 1/2$ in the mean field. Of course in the regime of critical fluctuations this exponent is corrected in both nonchiral [15] and chiral [17] universality classes.

Local terms in the GL energy density are also calculable exactly (within our approximation, see Appendix C):

$$f_{\text{cond}} = \frac{1}{4\pi\hbar^2 v_F^2} \left\{ -U \Delta^* \Delta + \frac{2}{3} (\Delta^* \Delta)^{3/2} \right\}. \tag{23}$$

It is quite nonstandard compared to the customary quartic term $(\Delta^* \Delta)^2$ in conventional universality classes. The GL equations in the homogeneous case for the condensate give $\Delta_0 = U^\beta$ with critical exponent $\beta = 1$, different from the mean-field value $\beta = 1/2$ for the $U(1)$ universality class [15]. The condensation energy density is $f_0 = -\frac{1}{12\pi\hbar^2 v_F^2} U^{2-\alpha}$ with $\alpha = -1$. The free-energy critical exponent at the QCP therefore is also different from the classical $\alpha = 0$.

Having calculated both the local terms and the momentum dependence of the quadratic term in the Ginzburg-Landau energy, one is ready to formulate the GL energy in an inhomogeneous situation including the magnetic field.

B. GL equations in the presence of magnetic field

In view of the local gauge invariance principle, replacing the momentum by a covariant derivative, the gradient term of the GL energy becomes

$$F_{\text{grad}} = \int d^2\mathbf{r} \frac{1}{16 v_F \hbar} \Delta^*(\mathbf{r}) \sqrt{\left[-i\partial_i - \frac{e^*}{c\hbar} A_i(\mathbf{r}) \right]^2} \Delta(\mathbf{r}). \tag{24}$$

This should be supplemented by the condensation energy Eq. (23) and magnetic energy Eq. (3). The GL equations are obtained by minimization with respect to the 2D order parameter and 3D vector potential. In the present case the equation for the order parameter is nonlocal and nonanalytic:

$$\left\{ \xi \sqrt{\left(-i\partial_i - \frac{e^*}{\hbar c} A_i \right)^2} - 1 \right\} \Delta + \frac{\Delta}{U} (\Delta^* \Delta)^{1/2} = 0. \tag{25}$$

The supercurrent in the Maxwell equation,

$$\frac{c}{4\pi} \nabla \times \mathbf{B} = \mathbf{J}(\mathbf{r}) \delta(z), \tag{26}$$

is also nonlocal: $J_i(\mathbf{r}) = \frac{1}{c} \frac{\delta F}{\delta A_i(\mathbf{r})}$.

C. Upper critical field and the magnetization curve

The upper critical field is found from the spectrum of the gradient term operator in Eq. (25). The lowest eigenvalue of the operator for homogeneous induction $\mathbf{B} = \{0,0,B\}$ is $\xi\sqrt{e^* B/c\hbar}$ (the eigenvalue of the square root of an operator is a square root of the eigenvalue), and therefore the bifurcation occurs at

$$H_{c2} = \frac{\Phi_0}{2\pi\xi^2}, \tag{27}$$

with the coherence length ξ found in Sec. II, Eq. (22). The formula is the same as in a more customary situation despite the fact that the coherence length has a different origin and different critical exponent at QCP.

Near H_{c2} the Abrikosov hexagonal lattice is formed. Its energy density is approximated well using the lowest Landau level (LLL) approximation: $\Delta(\mathbf{r}) = \Delta_A \varphi(\mathbf{r})$, where the Abrikosov hexagonal lattice function φ is normalized by $\langle |\varphi(\mathbf{r})|^2 \rangle = 1$ ($\langle ... \rangle$ denotes here the space average). The strength of the condensate is determined by minimizing the energy (magnetic energy can be neglected):

$$\begin{aligned} \langle f \rangle &= \frac{|\Delta_A|^2}{16 v_F \hbar} \left\langle \varphi^* \left\{ \sqrt{\left[-i\partial_i - \frac{e^*}{c\hbar} A_i(\mathbf{r}) \right]^2} - \frac{4U}{\pi v_F \hbar} \right\} \varphi \right\rangle \\ &\quad + \frac{|\Delta_A|^3}{6\pi\hbar^2 v_F^2} \langle |\varphi|^3 \rangle \\ &= -\frac{|\Delta_A|^2}{32 v_F \hbar} \sqrt{\frac{e^*}{c\hbar}} H_{c2}^{1/2} (1 - H/H_{c2}) + \frac{\beta_3 |\Delta_A|^3}{6\pi\hbar^2 v_F^2}. \end{aligned} \tag{28}$$

The number $\beta_3 = \langle |\varphi|^3 \rangle = 1.07$ is analogous to β_A for usual fourth power GL energy. The optimal Δ_A at external field H close to H_{c2} is

$$|\Delta_A| = \frac{U}{2\sqrt{2\pi}\beta_3} (1 - H/H_{c2})^\sigma, \quad \sigma = 1. \tag{29}$$

This exponent for the transition on the H_{c2} line is different from the ordinary Abrikosov lattice [22], for which $\sigma = 1/2$.

The magnetization, calculated from the averaged energy density for the optimal Δ_A given in Eq. (29), is ($B \simeq H$)

$$f(B) = -\frac{\sqrt{2\pi}}{3 \times 2^{10} \beta_3} \frac{U H_{c2}}{\Phi_0} (1 - H/H_{c2})^3. \tag{30}$$

The dependence is quadratic:

$$M = -\frac{\pi^{3/2}}{2^7\sqrt{2}\beta_3}\frac{U}{\Phi_0}(1 - H/H_{c2})^\tau, \tau = 2, \quad (31)$$

which should be contrasted with the usual linear dependence [22], $\tau = 1$. For smaller fields the vortex lattice becomes less dense and eventually the LLL approximation [23] breaks down. However, since the superconductivity is confined to an atomic-width layer, there is no H_{c1}, and at small fields vortices become independent. Consequently the parabolic increase is halted and perfect diamagnetism appears only at $H = 0$. Under these conditions we turn to a single vortex solution next.

D. Core structure of a single vortex

The single vortex solution for the order parameter can be found using the rotational symmetry in polar coordinates: $\Delta = Uf(r)e^{i\phi}$ with the homogeneous condensate value $\Delta = U$ found in Sec. II, so that at large distances the dimensionless order parameter $f(r) \to 1$. At the center of the vortex, f vanishes. The effects of the magnetic field, other than the phase rotation, are small in this extreme type-II case of a surface superconductor [22]. In this case the GL equation Eq. (25), using the coherence length ξ, Eq. (22) as the unit of length, and $\mathbf{r} \to \xi\mathbf{r}$, takes the form

$$(\sqrt{\widehat{L}} - 1)f(r) + f(r)^2 = 0. \quad (32)$$

The operator $\widehat{L} \equiv -\partial_r^2 - \frac{1}{r}\partial_r + \frac{1}{r^2}$ has Bessel functions as its eigenvectors:

$$\left(-\partial_r^2 - \frac{1}{r}\partial_r + \frac{1}{r^2}\right) J_1(\alpha r) = \alpha^2 J_1(\alpha r). \quad (33)$$

Looking for the solution expanded in the full set of these functions for all α satisfying our boundary conditions (Hankel transform) in the form

$$f(r) = 1 - \int_{\alpha=0}^{\infty} \alpha F(\alpha) J_1(\alpha r), \quad (34)$$

the equation becomes

$$\int_{\alpha=0}^{\infty} F(\alpha)\alpha(\alpha+1)J_1(\alpha r) = \left(\int_{\beta=0}^{\infty} \beta F(\beta) J_1(\beta r)\right)^2. \quad (35)$$

To obtain an iterative form we multiply by $rJ_1(\gamma r)$, and integrating over r using explicit formulas [24] given in Appendix D results in

$$F(\gamma) = \frac{1}{\pi(\gamma+1)}\int_{\alpha,\beta=0}^{\infty} \frac{F(\alpha)F(\beta)(\alpha^2+\beta^2-\gamma^2)}{\sqrt{[\gamma^2-(\alpha-\beta)^2][(\alpha+\beta)^2-\gamma^2]}}. \quad (36)$$

The iteration converges very fast with the result presented in Fig. 5 (dots). The asymptotic at small r is linear, $f(r) = r$, while at large r as expected it approaches the "bulk" value $f(r) \to 1$ and can be approximated by a formula $f(r) = \frac{r}{r+1}$ (the green curve in Fig. 5), simpler than the usual interpolation formula, $f(r) = \frac{r}{\sqrt{1+2r^2}}$ (the orange curve in Fig. 5). One observes that the relaxation of the order parameter away from the center of the vortex is much slower in the STI.

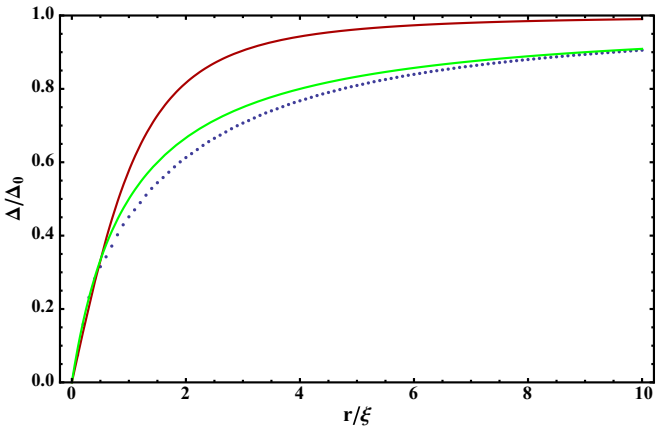

FIG. 5. (Color online) Vortex core structure near the QCP and order parameter in units of the bulk gap Δ_0 as a function of distance from the center in units of coherence length ξ. The dash line is the approximate formula, while the top line (red) is the usual Abrikosov vortex profile.

IV. DISCUSSION AND CONCLUSIONS

A. Comparison of renormalization of the coupling with BEC and BCS in two dimensions

Let us contrast the coupling renormalization in a 2D Weyl semimetal with momentum cutoff Λ (for definiteness one can assume the phonon mechanism so that Λ is the Debye cutoff T_D, under the condition that the deviation from the Weyl point $\mu \ll T_D$) with that in a 2D parabolic band, $E_p = \frac{p^2}{2m^*}$. The renormalized coupling, Eqs. (14) and (15), can be written in the form

$$\frac{1}{g_{\rm ren}} = \frac{1}{g} - \frac{\Lambda}{4\pi\hbar^2 v_F}, \quad (37)$$

where $g_{\rm ren} \equiv -4\pi\hbar^2 v_F^2/U$. The linear renormalization (rather than the customary logarithmic cutoff dependence) of $\frac{1}{g}$ in a Weyl semimetal is pertinent to the so-called "chiral universality classes" that sometimes appear in description of quantum critical points in two dimensions [14]. It corresponds to finite coupling g_c fixed points in Eqs. (14) and (15). This is the main difference from the more conventional cases that are briefly summarized next.

Within the parabolic case two cases are generally distinguished [25]: the BCS, where the chemical potential μ is well above the bottom of the band (see Fig. 6) so that $T_D \ll \mu$ (like in metallic superconductors), and the BEC when $\Lambda^2/2m^* \gg \mu$ (like in cold atoms).

In the BEC, that is closer to the STI considered here, the gap equation reads

$$\frac{1}{g^{\rm BEC}} = \frac{1}{2\pi}\int_{k=\hbar/L}^{\Lambda} \frac{k}{\sqrt{(k^2/2m^* - \mu)^2 + \Delta^2}} = \frac{m^*}{4\pi\hbar^2}\log\frac{\Lambda^2}{m^*\left(\sqrt{\mu_{\rm ren}^2 + \Delta^2} - \mu_{\rm ren}\right)}. \quad (38)$$

Here L is an infrared cutoff (needed in two dimensions) that is incorporated in $\mu_{\rm ren} = \mu - \frac{\hbar^2}{2L^2m^*}$. The corresponding renormalized coupling depends on the reference (normalization)

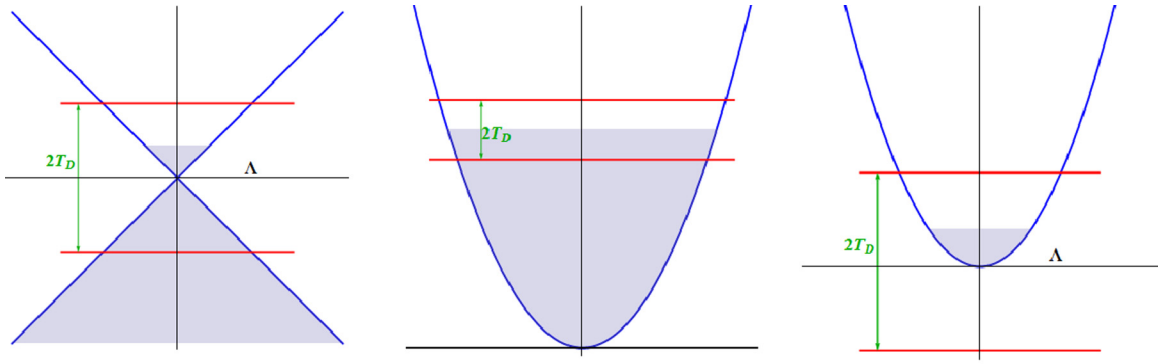

FIG. 6. (Color online) Schematic picture of the band reconstruction due to phonon pairing in three different 2D fermionic systems. (a) Weyl semimetal. (b) BCS with parabolic dispersion law. (c) Classic BEC.

point $E_{\rm ren}$ [26]:

$$\frac{1}{g_{\rm ren}^{\rm BEC}} = \frac{1}{g^{\rm BEC}} - \frac{m^*}{4\pi\hbar^2}\log\frac{\Lambda^2}{m^* E_{\rm ren}}. \tag{39}$$

In terms of this coupling the theory becomes cutoff independent. For example, the gap equation reads

$$\frac{1}{g_{\rm ren}^{\rm BEC}} = \frac{m^*}{4\pi\hbar^2}\log\frac{E_{\rm ren}}{\sqrt{\mu_{\rm ren}^2+\Delta^2}-\mu_{\rm ren}}. \tag{40}$$

In the BCS the gap equation, under the simplifying conditions $\mu \gg T_D > \Delta$ (the dispersion relation near the Fermi level can be approximated by a "flat" one [21]), is

$$\frac{1}{g^{\rm BCS}} = \frac{1}{2\pi}\int_{k=\sqrt{2m^*(\mu-T_D)}}^{\sqrt{2m^*(\mu+T_D)}} \frac{k}{\sqrt{(k^2/2m^*-\mu)^2+\Delta^2}} \simeq \frac{m^*}{2\pi\hbar^2}\log\frac{2T_D}{\Delta}. \tag{41}$$

The renormalized coupling is again dependent on an arbitrarily chosen normalization scale, $E_{\rm ren}$:

$$\frac{1}{g_{\rm ren}^{\rm BCS}} = \frac{1}{g^{\rm BCS}} - \frac{m^*}{2\pi\hbar^2}\log\frac{T_D}{E_{\rm ren}}.$$

In both parabolic cases the coupling is logarithmically "running" toward weak coupling [26] $g^{\rm BCS} \to g_c = 0$ (marginally irrelevant or asymptotically free) at large Λ. In the Weyl semimetal (where the dispersion is linear) with local interaction the criticality appears at small U when g approaches finite value g_c. Despite the fact that the UV cutoff does not appear logarithmically, the theory is still renormalizable [16] and any physical quantity can be expressed via renormalized coupling U.

B. Criticality beyond the Gaussian approximation

Critical (quantum) fluctuations are expected to be significant in this relatively low-dimensional (relativistic 2+1-dimensional) system. Generally they are not as strong as in a 2D statistical system at finite temperature but stronger than in a 3D one. The approximation we made describes reasonably well "Gaussian" fluctuation beyond the region where stronger critical fluctuations in these systems appear and should be treated nonperturbatively [16] typically using variants of the renormalization-group (RG) approach. The critical exponents in this region differ from the one called "quantum gaussian (BCS)" in [14], and available results are obtained using either ε expansion [27,28] ($\varepsilon = 4-d$, where $d = 2+1$ is the space-time dimension); $1/N$, where N is the number of fermionic species on the surface [17]; or functional (strong-coupling) RG [29] and Monte Carlo simulations [30,31] (with reservations specified below). The universality class according to classification proposed in [17] is the chiral XY [symmetry of order parameter $U(1)$] with $N = 1$. The large N expansion is not reliable for the one component system considered here (but the number might be larger in similar systems for which our approach trivially generalizes), so let us use the ε expansion.

Using the formulas for the anomalous dimensions of the order parameter [27], $\gamma_\Delta = \eta = 1/4\varepsilon + 0.044\varepsilon^2 + O(\varepsilon^3) \approx 0.294$ and its square $\gamma_{\Delta^2} = (1+\sqrt{11})/10\varepsilon + 0.065\varepsilon^2 \simeq 0.43\varepsilon + 0.065\varepsilon^2$, critical exponents are obtained from the hyperscaling relations, $\alpha = 2 - d/(2-\gamma_{\Delta^2}) = (\varepsilon - 2\gamma_{\Delta^2})/(2-\gamma_{\Delta^2}) = -0.353$ and $\beta = (1+\gamma_\Delta)/2(2-\gamma_{\Delta^2}) = 0.515$, and can be compared with those in Table I.The exponents from the ε expansion were found to be consistent for larger values of N with the latest Monte Carlo simulations [31], while for

TABLE I. Critical exponents of the chiral universality class of the Abrikosov transition in external magnetic field at QCP.

Critical exponent	Order parameter	Coherence length	Energy	Temperature
QCP U_1 (1) definition	$\Delta \propto U^\beta$	$\xi = U^{-\nu}$	$f \propto U^{2-\alpha}$	$T_c \propto U^{z\nu}$
Quantum Gauss	$\beta = 1$	$\nu = 1$	$\alpha = -1$	$z\nu = 1$
Classical U (1) definition	$\Delta \propto (T_c - T)^\beta$	$\xi \propto (T_c - T)^{-\nu}$	$f \propto (T_c - T)^{2-\alpha}$	
Classical Gauss	$\beta = \frac{1}{2}$	$\nu = \frac{1}{2}$	$\alpha = 0$	

Ising (Z_2) and Heisenberg [SU (2)] chiral universality classes are consistent with the functional RG [29].

C. Experimental feasibility of the surface superconductivity due to phonon exchange

To estimate the pairing efficiency due to phonons, one should rely on recent studies of surface phonons in TIs [7]. The coupling constant in the Hamiltonian, Eq. (1), is obtained from the exchange of acoustic (Rayleigh) surface phonons $g = \lambda v_F^2 \hbar^2 / 2\pi\mu$, where λ is the dimensionless effective electron-electron interaction constant of order 0.1 (somewhat lower values are obtained in [32]). It was shown in [7] that at zero temperature the ratio of λ and μ is constant with a well-defined $\mu \to 0$ limit with value $g = 0.23\text{eV nm}^2$ for $v_F \approx 7 \times 10^5$ m/s (for Bi_2Se_3). The critical coupling constant g_c, Eq. (15), can be estimated from the Debye cutoff $T_D = 200$ K determining the momentum cutoff $\Lambda = T_D/c_s$, where c_s is the sound velocity. Taking the value to be $c_s = 2 \times 10^3$ m/s (for Bi_2Se_3), one obtains $g_c = 4\pi v_F c_s \hbar^2 / T_D = 0.20\,\text{eV nm}^2$. Therefore the stronger superconductivity, $g > g_c$, is realized (see Fig. 3 and case 1 of Sec. II C, $U > 0$). Note that the superconductivity appears even for $0 < g < g_c$ ($U > 0$ in Fig. 3), although, as discussed in Sec. II C case 2, it is weaker.

Of course the Coulomb repulsion might weaken or even overpower the effect of the attraction due to phonons, so that superconductivity does not occur. In a TI like Bi_2Se_3, however, the dielectric constant is very large, $\varepsilon = 50$, so that the Coulomb repulsion is weak. Moreover it was found in graphene (that has identical Coulomb interaction) that, although the semimetal does not screen [20], the effects of the Coulomb coupling are surprisingly small, even in leading order in perturbation theory.

Superconductivity was observed in otherwise nonsuperconducting TIs Bi_2Te_3 and Bi_2Se_3. It was noticed very recently [6,33] that Bi nanoclusters naturally aggregate on the surface of Bi_2Te_3 thin film, and an explanation was put forward that the nanoclusters become superconducting and induce surface superconductivity in TIs by the proximity effect. We speculate that the nanoclusters are not superconducting and their role might be to screen the Coulomb repulsion.

In this paper we focused on the qualitatively distinct case of Weyl fermions with small chemical potential. Although in the original proposal of TIs in materials [8] the chemical potential was zero, in experiments one finds often that the Dirac point is shifted away from the Fermi surface by a significant fraction of eV [1]. There are, however, experimental methods to shift the location of the point by doping, gating, pressure, etc. [9]. Note that a reasonable electron density of $n = 3 \times 10^{11}$ cm^{-2} in Bi_2Te_3 already conforms to the requirement that chemical potential $\mu = \sqrt{n}\hbar v_F / 2\pi = 100$ K is smaller than the Debye cutoff energy $T_D = 200$ K.

V. CONCLUSIONS

We have studied the s-wave pairing on the surface of a 3D topological insulator. The noninteracting system is characterized by (nearly) zero density of states on the 2D Fermi manifold. It degenerates into a point when the chemical potential coincides with the Weyl point of the surface states as in the original proposal for a major class of such materials [8]. The pairing attraction (the most plausible candidate being surface phonons) therefore has two tasks in order to create the superconducting condensate. The first is to create a pair of electrons (that in the present circumstances means creating two holes as well), and the second is to pair them. To create the charges does not cost much energy since the spectrum of the Weyl semimetal is gapless (massless relativistic fermions); this is effective as long as the coupling g is larger than the critical g_c [see Eq. (15)]. The situation is more reminiscent of the creation of the chiral condensate in relativistic massless four-fermion theory (a 2D version [16] was recently contemplated for graphene [19,20]) than of the BCS or even BEC in condensed-matter systems with parabolic dispersion law. Due to the special ultrarelativistic nature of the pairing, transition at zero temperature as a function of parameters like the pairing interaction strength is unusual: even the mean-field critical exponents are different from the standard ones that generally belong to the U (1) class of second-order phase transitions.

TABLE II. Critical exponents of the chiral universality class of the TI QCP.

Critical exponent	Magnetization	OP magnetic
QCP $U_1(1)$ definition	$M \propto (H_{c2} - H)^\tau$	$\Delta_A \propto (H_{c2} - H)^\sigma$
Quantum Gauss	$\tau = 2$	$\sigma = 1$
Abrikosov lattice definition	$M \propto (H_{c2} - H)^\tau$	$\Delta_A \propto (H_{c2} - H)^\sigma$
Classical Gauss	$\tau = 1$	$\sigma = \frac{1}{2}$

To summarize, we calculated, using the Gor'kov theory, the phase diagram of the superconducting transition at arbitrary chemical potential μ, effective coupling energy U, and temperature T (see Figs. 2 and 3). The quantum ($T = 0$) critical point appears at $\mu = 0, U = 0$ and belongs to the U_1 (1) *chiral* universality class (the subscript denotes the number of massless fermions at the QCP) according to classification in [14,17]. The critical exponents are summarized in Table I for the "static" exponents and in Table II for response to temperature and magnetic field (gauge coupling). The Ginzburg-Landau effective theory near the QCP, Eq. (25), was derived and is rather unusual. The magnetization curve near H_{c2} due to the vortex lattice is parabolic rather than linear. This might be important for experimental identification of the QCP. The vortex core structure was determined (see Fig. 5) and has some peculiarities that can be tested directly.

ACKNOWLEDGMENTS

We are indebted to C. W. Luo, J. J. Lin, and W. B. Jian, for explaining details of experiments, and to T. Maniv and M. Lewkowicz for valuable discussions. The work of D.L. and B.R. was supported by the National Science Council of the Republic of China Grant No. 98-2112-M-009-014-MY3 and the Ministry of Education ATU program. The work of D.L. also is supported by the National Natural Science Foundation of China (Grant No. 11274018).

APPENDIX A: INTEGRALS AND SUMS FOR GAP EQUATION

The bubble integral in the gap equation Eq. (10) at finite temperature can be written as

$$b = \frac{T}{2}\sum_{n,\mathbf{p}}\left\{\frac{1}{\Delta^2+\hbar^2\omega_n^2+(v_F p+\mu)^2}\right. \tag{A1}$$

$$\left.+\frac{1}{\Delta^2+\hbar^2\omega_n^2+(v_F p-\mu)^2}\right\}. \tag{A2}$$

At zero temperature after integration over frequencies, it becomes (summation over momenta is replaced by the integral with momentum cutoff Λ in polar coordinates)

$$b = \frac{1}{8\pi\hbar^2}\int_{p=0}^{\Lambda} p\left\{\frac{1}{\sqrt{\Delta^2+(v_F p+\mu)^2}}\right. \tag{A2}$$

$$\left.+\frac{1}{\sqrt{\Delta^2+(v_F p-\mu)^2}}\right\}. \tag{A3}$$

The integral is readily performed and expanded in $1/\Lambda$:

$$\begin{aligned} b &= \frac{1}{8\pi\hbar^2 v_F^2}\left\{\sqrt{\Delta^2+(v_F\Lambda+\mu)^2}+\sqrt{\Delta^2+(v_F\Lambda-\mu)^2}\right.\\ &\left.+\mu\log\frac{(\sqrt{\Delta^2+\mu^2}+\mu)(v_F\Lambda-\mu+\sqrt{\Delta^2+(v_F\Lambda-\mu)^2})}{(\sqrt{\Delta^2+\mu^2}-\mu)(v_F\Lambda+\mu+\sqrt{\Delta^2+(v_F\Lambda+\mu)^2})}-2\sqrt{\Delta^2+\mu^2}\right\}\\ &\simeq \frac{1}{4\pi\hbar^2 v_F^2}\left\{v_F\Lambda\ -\sqrt{\Delta^2+\mu^2}+\frac{\mu}{2}\log\frac{\mu+\sqrt{\Delta^2+\mu^2}}{\sqrt{\Delta^2+\mu^2}-\mu}\right\}+O\left(\frac{1}{\Lambda}\right). \end{aligned} \tag{A4}$$

At finite temperature, using the sum,

$$T\sum_n(\omega_n^2+m^2)^{-1} = \frac{\tanh[m/(2T)]}{2m}, \tag{A5}$$

one obtains

$$B = \frac{1}{8\pi}\int_{p=0}^{\Lambda} p\left\{\frac{\tanh[\sqrt{\Delta^2+(v_F p+\mu)^2}/(2T)]}{\sqrt{\Delta^2+(v_F p+\mu)^2}}\right. \tag{A6}$$

$$\left.+\frac{\tanh[\sqrt{\Delta^2+(v_F p-\mu)^2}/(2T)]}{\sqrt{\Delta^2+(v_F p-\mu)^2}}\right\}. \tag{A7}$$

For $\mu = 0$ it simplifies:

$$\begin{aligned} b &= \frac{1}{4\pi\hbar^2}\int_{p=0}^{\Lambda} p\frac{\tanh\left[\sqrt{\Delta^2+v_F^2p^2}/(2T)\right]}{\sqrt{\Delta^2+v_F^2p^2}}\\ &= \frac{1}{4\pi\hbar^2 v_F^2}\left\{v_F\Lambda-2T\log\left[2\cosh\left(\frac{\Delta}{2T}\right)\right]\right\}. \end{aligned} \tag{A8}$$

This was used in Eq. (18). For $\Delta = 0$ and $\mu \neq 0$,

$$b = \frac{1}{8\pi\hbar^2}\int_{p=0}^{\Lambda} p\left\{\frac{\tanh[|v_F p+\mu|/(2T_c)]}{|v_F p+\mu|}\right. \tag{A9}$$

$$\left.+\frac{\tanh[|v_F p-\mu|/(2T_c)]}{|v_F p-\mu|}\right\}. \tag{A10}$$

APPENDIX B: CRITICAL LINE AND CONDENSATE

The dependence of the gap on chemical potential is given in Eq. (11). For positive U and $\mu \ll \Delta$ the formula can be expanded as

$$U = \sqrt{\Delta^2+\mu^2}-\frac{\mu}{2}\log\frac{\sqrt{\Delta^2+\mu^2}+\mu}{\sqrt{\Delta^2+\mu^2}-\mu} = \Delta-\frac{\mu^2}{2\Delta}, \tag{B1}$$

from which Eq. (17) follows. In the case of $U = 0$ the equation becomes homogeneous:

$$\sqrt{\Delta^2+\mu^2} = \frac{\mu}{2}\log\frac{\sqrt{\Delta^2+\mu^2}+\mu}{\sqrt{\Delta^2+\mu^2}-\mu} \to \frac{\Delta}{\mu} = 0.663. \tag{B2}$$

In the negative U case Δ is exponentially small (so that $\mu \gg \Delta$) and

$$\begin{aligned} U &= \sqrt{\Delta^2+\mu^2}-\frac{\mu}{2}\log\frac{\sqrt{\Delta^2+\mu^2}+\mu}{\sqrt{\Delta^2+\mu^2}-\mu}\\ &\simeq \mu-\mu\log\frac{\mu}{\Delta}, \end{aligned} \tag{B3}$$

from which Eq. (16) follows. The critical temperature for arbitrary μ is obtained as the $\Delta \to 0$ limit of the gap equation Eq. (18):

$$U = \frac{v_F}{2}\int_{p=0}^{\Lambda} p\left\{\frac{\tanh[|v_F p+\mu|/(2T_c)]}{|v_F p+\mu|}\right. \tag{B4}$$

$$\left.+\frac{\tanh[|v_F p-\mu|/(2T_c)]}{|v_F p-\mu|}-\frac{2}{|p|}\right\}. \tag{B5}$$

This is presented in Fig. 3.

APPENDIX C: DERIVATION OF THE GL ENERGY FOR AT QCP

1. Linear term in GL equation for arbitrary momentum p

Expanding the right-hand side of Eq. (10) to a linear term, the expression for the kernel can be written as a trace:

$$\begin{aligned} \Gamma &= \frac{1}{2}\mathrm{tr}\left\{\sum_{\omega q}\sigma^y D^t_{\omega q}\sigma^y D_{\omega,q-p}+\frac{1}{g}I\right\}\\ &= \frac{1}{g}-\sum_{\omega q}\frac{\hbar^2\omega^2-v_F^2pq+v_F^2q^2}{\left(\hbar^2\omega^2+v_F^2q^2\right)\left(\hbar^2\omega^2+v_F^2|\mathbf{q}-\mathbf{p}|^2\right)}. \end{aligned} \tag{C1}$$

Integrating over ω (at zero temperature) one obtains

$$\Gamma = -\frac{U}{4\pi\hbar^2 v_F^2} - \frac{1}{2v_F}\sum_q \frac{pq - p^2}{q\,(q-p)^2 + q^2\,|\mathbf{q}-\mathbf{p}|} = -\frac{1}{8\pi^2\hbar^2 v_F}\int_{q,\phi}\frac{pq\cos\phi - p^2}{|\mathbf{q}-\mathbf{p}|^2 + q\,|\mathbf{q}-\mathbf{p}|} - \frac{U}{4\pi\hbar^2 v_F^2}, \tag{C2}$$

where

$$|\mathbf{q}-\mathbf{p}|^2 = q^2 + p^2 - 2pq\cos\phi.$$

The integral is homogeneous in momentum and therefore is linear in $p = |\mathbf{p}|$, and one arrives at Eq. (21).

2. Local terms in GL equation and energy

For $p = 0$ the gap equation Eq. (13) reads

$$\frac{\Delta}{4\pi\hbar^2 v_F^2}(-U + \sqrt{\Delta^*\Delta}) = 0. \tag{C3}$$

This is obtained from the energy functional:

$$F = \frac{1}{4\pi\hbar^2 v_F^2}\int d^2\mathbf{r}\left\{-U\,\Delta^*\Delta + \frac{2}{3}(\Delta^*\Delta)^{3/2}\right\}. \tag{C4}$$

APPENDIX D: SINGLE VORTEX

The basic integral of the Hankel transform is

$$I_2 = \int_{r=0}^{\infty} r\,J_1(ar)\,J_1(br) = \delta(a-b)\,\frac{1}{a}. \tag{D1}$$

This has been generalized by Auluck [24] to three functions:

$$I_3 = \int_{r=0}^{\infty} r\,J_1(ar)J_1(br)J_1(cr) = \frac{\pi}{4c^2}\sin\phi\,P_1^{-1}(\cos\phi) = \frac{\pi}{4c^2}\sin^2\phi. \tag{D2}$$

Here $c < a+b$, $a < b+c$, $b < a+c$, and ϕ is the angle between sides a and b of the triangle formed by a, b, and c:

$$\sin^2\phi = \frac{[c^2-(a-b)^2][(a+b)^2-c^2]}{4a^2b^2}, \tag{D3}$$

and P is the Legendre spherical harmonic. Consequently,

$$I_3 = \pi\,\frac{[c^2-(a-b)^2][(a+b)^2-c^2]}{16a^2b^2c^2}. \tag{D4}$$

[1] X.-L. Qi and S.-C. Zhang, Rev. Mod. Phys. **83**, 1057 (2011).
[2] V. M. Nabutovskii and B. Ya. Shapiro, Zh. Eksp. Teor. Fiz. **84**, 422 (1983) [Sov. Phys. JETP **57**, 245 (1983)].
[3] P. A. Lee, N. Nagaosa, and X.-G. Wen, Rev. Mod. Phys. **78**, 17 (2006); J. Orenstein and A. J. Millis, Science **288**, 468 (2000).
[4] J. Singleton and C. Mielke, Cont. Phys. **43**, 63 (2002).
[5] I. N. Khlyustikov and A. I. Buzdin, Adv. Phys. **36**, 271 (1987).
[6] X. Zhu, L. Santos, R. Sankar, S. Chikara, C. Howard, F. C. Chou, C. Chamon, and M. El-Batanouny, Phys. Rev. Lett. **107**, 186102 (2011); C. W. Luo, H. J. Wang, S. A. Ku, H.-J. Chen, T. T. Yeh, J.-Y. Lin, K. H. Wu, J. Y. Juang, B. L. Young, T. Kobayashi, C.-M. Cheng, C.-H. Chen, K.-D. Tsuei, R. Sankar, F. C. Chou, K. A. Kokh, O. E. Tereshchenko, E. V. Chulkov, Yu. M. Andreev, and G. D. Gu, Nano Lett. **13**, 5797 (2013); X. Zhu, L. Santos, C. Howard, R. Sankar, F. C. Chou, C. Chamon, and M. El-Batanouny, Phys. Rev. Lett. **108**, 185501 (2012).
[7] S. Das Sarma and Qiuzi Li, Phys. Rev. B **88**, 081404(R) (2013).
[8] H. Zhang, C.-X. Liu, X.-L. Qi, X. Dai, Z. Fang, and S.-C. Zhang, Nat. Phys. **5**, 438 (2009).
[9] J. G. Checkelsky, Y. S. Hor, R. J. Cava, and N. P. Ong, Phys. Rev. Lett. **106**, 196801 (2011); D. Kim, S. Cho, N. P. Butch, P. Syers, K. Kirshenbaum, S. Adam, J. Paglione, and M. S. Fuhrer, Nat. Phys. **8**, 459 (2012).
[10] I. F. Herbut and C.-K. Lu, Phys. Rev. B **82**, 125402 (2010).
[11] A. L. Rakhmanov, A. V. Rozhkov, and F. Nori, Phys. Rev B **84**, 075141 (2011).
[12] M. Cheng, R. M. Lutchyn, and S. Das Sarma, Phys. Rev B **85**, 165124 (2012).
[13] M. Sato and S. Fujimoto, Phys. Rev B **79**, 094504 (2009).
[14] S. Sachdev, *Quantum Phase Transitions*, 2nd ed. (Cambridge University Press, Cambridge, 2011).
[15] L. D. Landau and E. M. Lifshitz, *Statistical Physics* (Pergamon, Oxford, 1980), Vol. 1.
[16] B. Rosenstein, B. J. Warr, and S. H. Park, Phys. Rev. Lett. **62**, 1433 (1989); Phys. Reports **205**, 59 (1991).
[17] G. Gat, A. Kovner, and B. Rosenstein, Nucl. Phys. B **385**, 76 (1992).
[18] R. Schneider, A. G. Zaitsev, D. Fuchs, and H. v. Löhneysen, Phys. Rev. Lett. **108**, 257003 (2012).
[19] O. V. Gamayun, E. V. Gorbar, and V. P. Gusynin, Phys. Rev. B **81**, 075429 (2010); B. Rosenstein and B. J. Warr, Phys. Lett. B **218**, 465 (1989); I. F. Herbut, V. Juricic, and B. Roy, Phys. Rev. B **79**, 085116 (2009); B. Roy and I. F. Herbut, *ibid.* **82**, 035429 (2010); M. V. Ulybyshev, P. V. Buividovich, M. I. Katsnelson, and M. I. Polikarpov, Phys. Rev. Lett. **111**, 056801 (2013).
[20] V. N. Kotov, B. Uchoa, V. M. Pereira, F. Guinea, and A. H. Castro Neto, Rev. Mod. Phys. **84**, 1067 (2012).
[21] A. A. Abrikosov, L. P. Gor'kov, and I. E. Dzyaloshinskii, *Quantum Field Theoretical Methods in Statistical Physics* (Pergamon, New York, 1965).
[22] A. A. Abrikosov, Zh. Eksp. Teor. Fiz. **32**, 1442 (1957) [Sov. Phys. JETP **5**, 1174 (1957)]; J. D. Ketterson and S. N. Song, *Superconductivity* (Cambridge University, Cambridge, 1999).
[23] B. Rosenstein and D. Li, Rev. Mod. Phys. **82**, 109 (2010).
[24] S. K. H. Auluck, Mathematica J. **14**, 1 (2012).
[25] H. T. C. Stoof, K. B. Gubbels, and D. B. M. Diskerscheid, *Ultracold Quantum Fields* (Springer Science, Dordrecht, The Netherlands, 2009).
[26] R. Shankar, Rev. Mod. Phys. **66**, 129 (1994).
[27] B. Rosenstein, H.-L. Yu, and A. Kovner, Phys. Lett. B **314**, 381 (1993).
[28] I. F. Herbut, V. Juricic, and O. Vafek, Phys. Rev. B **80**, 075432 (2009); B. Roy, V. Juričić, and I. F. Herbut, *ibid.* **87**, 041401 (2013).
[29] L. Janssen and I. F. Herbut, Phys. Rev. B **89**, 205403 (2014).

[30] L. Del Debbio, S. J. Hands, and J. C. Mehegan, Nucl. Phys. B **502**, 269 (1997); I. M. Barbour, N. Psycharis, E. Focht, W. Franzki, and J. Jersak, Phys. Rev. D **58**, 074507 (1998).

[31] S. Chandrasekharan and A. Li, Phys. Rev. D **85**, 091502 (2012); S. Chandrasekharan, *ibid.* **86**, 021701(R) (2012); S. Chandrasekharan and A. Li, *ibid.* **88**, 021701(R) (2013).

[32] Z.-H. Pan, A. V. Fedorov, D. Gardner, Y. S. Lee, S. Chu, and T. Valla, Phys. Rev. Lett. **108**, 187001 (2012); V. Parente, A. Tagliacozzo, F. von Oppen, and F. Guinea, Phys. Rev. B **88**, 075432 (2013).

[33] G. Koren, T. Kirzhner, E. Lahoud, K. B. Chashka, and A. Kanigel, Phys. Rev. B **84**, 224521 (2011).